Draft version May 2, 2016
Preprint typeset using LaTeX style emulateapj v. 5/2/11

arXiv:1604.08710v1 [astro-ph.HE] 29 Apr 2016

FERMI STUDY OF γ-RAY MILLISECOND PULSARS: THE SPECTRAL SHAPE AND PULSED 25–200 GEV EMISSION FROM J0614−3329

Yi Xing and Zhongxiang Wang
Key Laboratory for Research in Galaxies and Cosmology, Shanghai Astronomical Observatory,
Chinese Academy of Sciences, 80 Nandan Road, Shanghai 200030, China

Draft version May 2, 2016

ABSTRACT

We report our analysis of the *Fermi* Large Area Telescope data for 39 millisecond pulsars (MSPs) listed in the second γ-ray pulsar catalog. Spectra of the pulsars are obtained. We fit the spectra with a function of a power law with exponential cutoff, and find the best-fit parameters of photon index $\Gamma = 1.54^{+0.10}_{-0.11}$ and cutoff energy $E_c = 3.70^{+0.95}_{-0.70}$ GeV. This spectral shape, which includes the intrinsic differences in the spectra of the MSPs, can be used for finding candidate MSPs and unidentified types of sources detected by *Fermi* at high Galactic latitudes. In one of the MSPs PSR J0614−3329, we find significant pulsed emission upto 200 GeV. The result has thus added this MSP to the group of the Crab and Vela pulsars that have been detected with >50 GeV pulsed emission. Comparing the γ-ray spectrum of PSR J0614−3329 with those of the Crab and Vela pulsars, we discuss possible emission mechanisms for the very high-energy component.

Subject headings: gamma rays: stars — pulsars: general — pulsars: individual (PSR J0614−3329)

1. INTRODUCTION

Since the launch of *Fermi Gamma-Ray Space Telescope (Fermi)* in year 2008, the Large Area Telescope (LAT) onboard it has been scanning the whole sky with unprecedented sensitivity at 0.1–300 GeV energy range. Thus far, more than 3000 γ-ray sources have been observed at the γ-ray energy range (Acero et al. 2015), and we are able to study bright sources among them in great detail. From *Fermi* LAT observations, we have learned that pulsars are the prominent γ-ray sources in our Galaxy. More than 200 pulsars have been found with γ-ray emission, half of which are millisecond pulsars (MSPs; Abdo et al. 2013).[1] Emission from pulsars at the *Fermi* LAT energy range generally can be described by a power law with exponential cutoff, where the cutoff energy is in a range of 1–7 GeV (Abdo et al. 2013). This spectral feature, along with that of stable emission, can be used for finding good pulsar candidates among the unidentified γ-ray sources found by *Fermi*.

MSPs are $\sim 10^9$ yr old neutron stars, having evolved from low-mass X-ray binaries by gaining sufficient angular momentum from accretion (Alpar et al. 1982; Radhakrishnan & Srinivasan 1982). Because of their old ages, the γ-ray MSPs appear to be isotropically distributed in the sky (Abdo et al. 2013). The distribution makes them mixed with the extragalactic γ-ray sources, which include Active Galactic Nuclei (AGN; the major class of γ-ray sources in the sky), several other types of galaxies (Acero et al. 2015), and even possibly unidentified types of sources (e.g., Bertoni et al. 2015). With the release of *Fermi* LAT Pass 8 database in year 2015, the detection sensitivity has been improved significantly, particularly at the low and high end of the LAT energy range. More faint sources, in addition to $\sim$ 3000 sources reported in the LAT third source catalog Acero et al. (2015), appear in the data analysis. For the purpose of finding candidate MSPs (e.g., Dai et al. 2016), a fine definition for the spectral shape of γ-ray MSPs is needed.

We therefore have conducted analysis of the LAT data for 39 γ-ray MSPs reported in the second LAT catalog of γ-ray pulsars (hereafter 2PC). We have extracted their spectra in a uniform way by using the latest Pass 8 database, and obtained the general spectral shape from their spectra. In addition, our analysis has revisited the >10 GeV emission found in three MSPs by Ackermann et al. (2013), and in PSR J0614−3329, we have found significant upto 200 GeV emission. In this paper, we report these results.

2. *FERMI* LAT DATA

LAT is a γ-ray imaging instrument onboard *Fermi* that scans the whole sky every three hours and can continuously conduct long-term γ-ray observations of thousands of GeV sources (Atwood et al. 2009). In this analysis, we selected 39 of 40 MSPs listed in 2PC (Abdo et al. 2013) as our targets (see Table 1), while PSR J1939+2134 was not included because of the low detection significance for it ($\simeq 3\sigma$). The data we used for each target are the 0.1–300 GeV LAT events in the *Fermi* Pass 8 database inside a $20^o \times 20^o$ region centered at a target's position. To fully study the very high-energy emission from PSR J0614−3329, for the detailed data analysis for this MSP, the high-energy end was extended to 500 GeV. The time period of the LAT data is from 2008-08-04 15:43:36 (UTC) to 2016-01-28 00:08:16 (UTC). Following the recommendations of the LAT team[2], we included those events with zenith angles less than 90 degrees, which prevents the Earth's limb contamination, and excluded the events with quality flags of 'bad'. In our following analysis, the background Galactic and extragalactic diffuse emission of the spectral model gll_iem_v06.fits and the file iso_P8R2_SOURCE_V6_v06.txt, respectively, were used. The normalizations of the diffuse components

[1] https://confluence.slac.stanford.edu/display/GLAMCOG/Public+List+of+LAT-Detected+Gamma-Ray+Pulsars
[2] http://fermi.gsfc.nasa.gov/ssc/data/analysis/scitools/

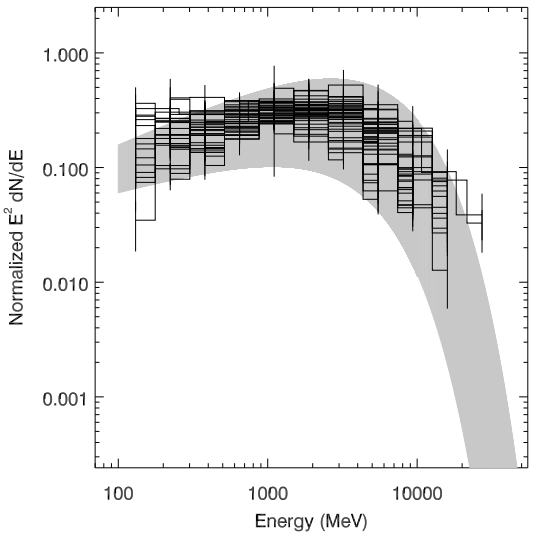

FIG. 1.— Normalized spectra of 39 MSPs. The uncertainties include the statistic and systematic ones (with the latter due to the Galactic diffuse emission model used). The grey area indicates the 3σ region of the best-fit spectral model.

in the analysis were always set as free parameters.

3. DATA ANALYSIS AND RESULTS FOR 39 MSPS

3.1. *Likelihood Analysis*

For each of the MSP targets, we included all sources within 20 degrees centered at their positions to make the source models based on the *Fermi* LAT 4-yr catalog (Acero et al. 2015). The spectral forms of these sources are provided in the catalog. Spectral parameters of the sources within 5 degrees from each target were set as free parameters, and the other parameters were fixed at their catalog values. The catalog spectral models for 33 MSPs are an exponentially cutoff power law, $dN/dE = N_0 E^{-\Gamma} \exp(-E/E_c)$, while for the other six MSPs (J0610−2100, J1446−4701, J1747−4036, J1125−5825, J1741+1351, and J1823−3021A) are a simple power law, $dN/dE = N_0 E^{-\Gamma}$.

Using the LAT science tools software package `v10r0p5`, we performed standard binned likelihood analysis to the LAT data of the MSP targets in the >0.1 GeV band. For PSRs J1658−5324 and J1858−2216, the analysis could not converge, which might be because of the relatively large uncertainties of the instrument response function of the LAT in the low energy range. We thus used >0.2 GeV data instead for the two sources. The spectral results as well as the Test Statistic (TS) values are given in Table 1 for each source. The TS value at a given position is calculated from TS= $-2\log(L_0/L_1)$, where L_0 and L_1 are the maximum likelihood values for a model without and with an additional source respectively. It is a measurement of the fit improvement for including the source, and is approximately the square of the detection significance of the source (Abdo et al. 2010).

For the 6 MSPs with a power-law spectral model in the catalog, we repeated the analysis with an exponentially cutoff power law. The significance of a spectral cutoff was estimated from $\sqrt{-2\log(L_{pl}/L_{exp})}$, where L_{exp} and L_{pl} are the maximum likelihood values when a target's emission was modeled with a power law with and without the cutoff respectively (Abdo et al. 2013). We found that for the 6 pulsars, the spectral cutoff was detected with $>3\sigma$ significance. Therefore in Table 1, we only provide the exponentially cutoff power-law results for them.

3.2. *Spectral Analysis*

We extracted the γ-ray spectra of the MSP targets by performing maximum likelihood analysis to the LAT data in 15 evenly divided energy bands in logarithm from 0.1–300 GeV. In the extraction, the spectral normalizations of the sources within 5 degrees from each target were set as free parameters, while all the other parameters of the sources were fixed at the values obtained from the above maximum likelihood analysis. The targets were considered as point sources having power-law emission with Γ fixed at 2.0. The fluxes obtained in this way are less dependent on the overall spectral model assumed for a source, providing a good description for the γ-ray emission of the source. We kept only flux data points when TS greater than 9 (i.e., $>3\sigma$ significance). A total of 304 data points were obtained for the 39 targets. The flux values for each target are provided in Table 2. We also estimated the systematic uncertainties caused by the Galactic diffuse emission model used. The uncertainty in each energy band was obtained by repeating the likelihood analysis with the normalization of the diffuse component artificially fixed to the values ±6% deviating from the best-fit value (see, e.g., Abdo et al. 2013). The uncertainties given in Table 2 have included the systematic uncertainties. We checked the spectrum and best-fit model for each target. The spectra are well fitted by the spectral models obtained from the likelihood analysis.

3.3. *Spectral Shape Determination*

In order to obtain a spectral shape that generally defines emission from MSPs, we first normalized the fluxes of each MSP target with its 0.1–300 GeV energy flux (F_{100} in Table 1). The normalized spectra of the 39 MSPs are shown in Figure 1. We then fit these data points with a normalized exponentially cutoff power law, i.e., N_0 is obtained from Γ and E_c by requiring the total flux to be 1. The best-fit values we obtained were $\Gamma = 1.5$ and $E_c = 3.8$ GeV, but with a minimum χ^2 value of 2198 for 302 degrees of freedom. The large χ^2 reflects the intrinsic spectral differences of the MSPs.

We thus used a systematic uncertainty parameter to represent the intrinsic differences. The parameter was added to the uncertainties of the data points in quadrature. We found that when this parameter was set to be 0.05, the minimum reduced χ^2 was approximately equal to 1. As a result, $\Gamma = 1.54^{+0.10}_{-0.11}$ and $E_c = 3.70^{+0.95}_{-0.70}$ GeV were obtained, where the uncertainties are at a 3σ confidence level. This 3σ spectral region is shown as the grey area in Figure 1.

4. DATA ANALYSIS AND RESULTS FOR PSR J0614−3329

In our analysis, we naturally revisited the high-energy >10 GeV emission from three MSPs found by Ackermann et al. (2013) in 2PC. In PSR J0614−3329, we found a significant high-energy component and thus conducted detailed analysis of the data for this pulsar.

4.1. *Timing Analysis*

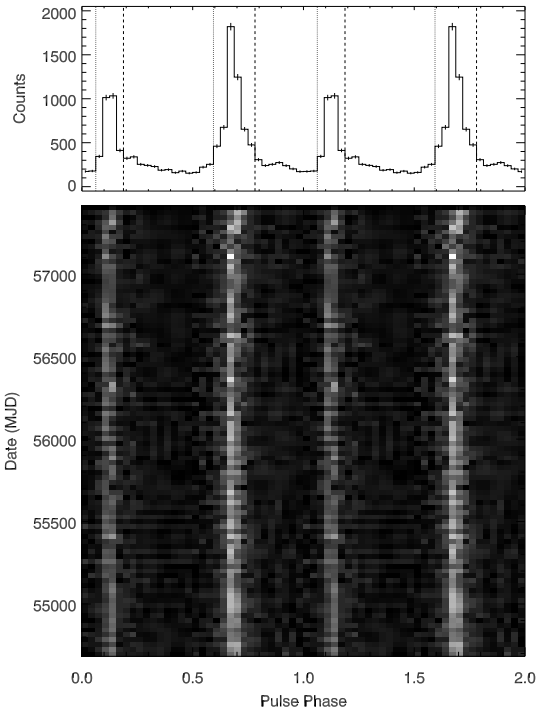

FIG. 2.— Folded pulse profile and two-dimensional phaseogram in 32 phase bins obtained for PSR J0614−3329. The grayscale represents the number of photons in each bin. The dotted and dashed lines mark the phase ranges defined for the on-pulse phase intervals. Two cycles are displayed for clarity.

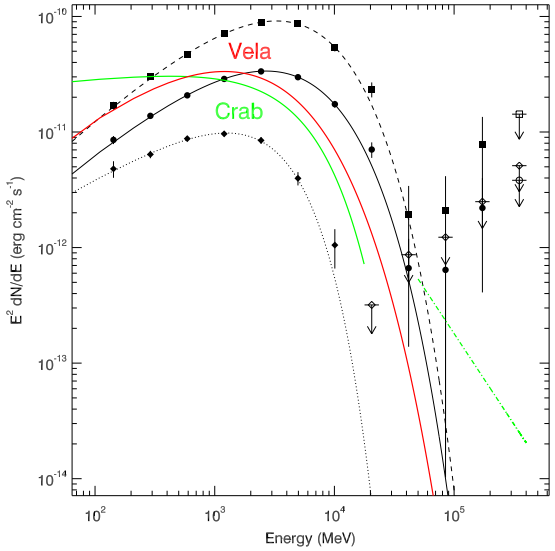

FIG. 3.— *Fermi* γ-ray spectra of PSR J0614−3329 during the total (dots), onpulse (squares), and offpulse (diamonds) phase intervals. The solid and dashed curves are the 0.1–500 GeV sub-exponentially cutoff power-law fits to emission during the total and onpulse phase intervals, respectively. The dotted curve is the 0.1–500 GeV exponentially cutoff power-law fit to emission during the offpulse phase intervals. The flux-scaled model fits to γ-ray emission of the Crab (Abdo et al. 2013; Aleksić et al. 2011) and Vela (Leung et al. 2014) pulsars are shown as green and red curves, respectively, for comparison.

We performed timing analysis to the 0.1–500 GeV LAT data of the PSR J0614−3329 region to update the γ-ray ephemeris given in Abdo et al. (2013). An aperture radius of 1.°0 was used. Pulse phases for photons before MJD 55797 (the end time of the known ephemeris) were assigned according to the known ephemeris using the *Fermi* plugin of TEMPO2 (Hobbs et al. 2006; Edwards et al. 2006). An 'empirical Fourier' template profile was built. Using this template, we generated the times of arrival (TOAs) of 40 evenly divided observations of the whole time period. Both the template and TOAs were obtained using the maximum likelihood method described in Ray et al. (2011).

We used TEMPO2 to fit the TOAs. Only the pulse frequency derivative $\dot{f}$ was fitted, and the other timing parameters were fixed to their known values. We obtained $\dot{f} = -1.7559(1) \times 10^{-15}\,\mathrm{s}^{-2}$, consistent with the value given in Abdo et al. (2013) within $\sim 2.2\sigma$ uncertainty. The folded pulse profile and two-dimensional phaseogram are shown in Figure 2. In the following analysis, we selected phase 0.06–0.19 and 0.59–0.78 as the onpulse phase intervals, and the rest as the offpulse phase intervals.

4.2. *Likelihood Analysis*

We included all sources within 20 degrees centered at the position of PSR J0614−3329 in the *Fermi* LAT 4-year catalog (Acero et al. 2015) to make the source model. The spectral forms of these sources are provided in the catalog. Spectral parameters of the sources within 5 degrees from PSR J0614−3329 were set as free parameters, and the other parameters were fixed at their catalog values. The catalog spectral form of PSR J0614−3329 is an exponentially cutoff power law, $dN/dE = N_0 E^{-\Gamma} \exp[-(E/E_c)^b]$. The parameter b is a measurement of the exponential cutoff shape, where a value of 1 or <1 indicates a simple exponential cutoff or a sub-exponential cutoff, respectively. We also used a simple power law in the analysis for comparison.

We performed standard binned likelihood analysis to the LAT data in >0.1 GeV energy range. We first set $b = 1$. The γ-ray emission during the total pulse phase intervals was detected with a TS value of 33576, while that during the onpulse and offpulse phase intervals were detected with TS values of 37013 and 3766, respectively. We found that during the total, onpulse, and offpulse phase intervals, the emission was better modeled with an exponentially cutoff power law. The cutoffs were significantly detected during all the three phase intervals ($> 5\sigma$; estimated from $\sqrt{-2\log(L_{pl}/L_{exp})}$). The resulting power-law fits with simple exponential cutoff are summarized in Table 3.

We then set b as a free parameter and repeated the binned likelihood analysis to the LAT data. We found that during the total and onpulse phase intervals the sub-exponential cutoffs were detected with $\sim 4\sigma$ significance (estimated from $\sqrt{-2\log(L_{exp}/L_{subexp})}$, where L_{subexp} is the maximum likelihood value for the sub-exponentially cutoff power-law model; Abdo et al. 2013). The resulting sub-exponentially cutoff power-law fits during these two phase intervals are given in Table 3. During the offpulse phase interval, the sub-exponential cutoff was not detected, as the detection significance was approximately zero.

4.3. *Spectral Analysis*

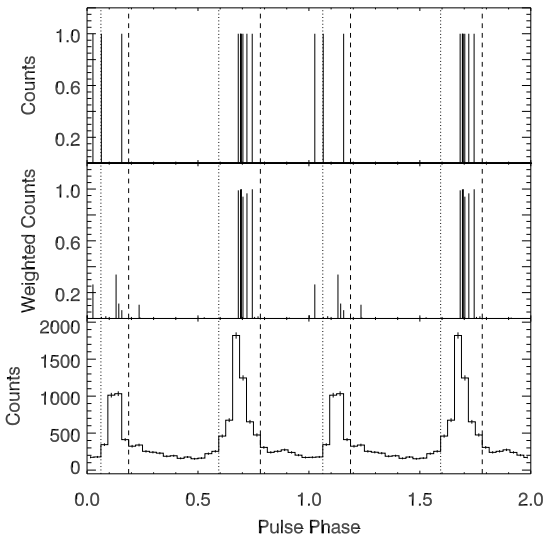

FIG. 4.— *Top* panel: >25 GeV photons within 0.°5 from PSR J0614−3329. *Middle* panel: weighted >25 GeV photons within 2° from PSR J0614−3329. *Bottom* panel: 0.1–500 GeV folded pulse profile in 32 phase bins obtained for PSR J0614−3329. The dotted and dashed lines mark the phase ranges for the on-pulse phase intervals. Two cycles are displayed for clarity.

We extracted the γ-ray spectra of PSR J0614−3329 during the total, onpulse, and offpulse phase intervals, by performing maximum likelihood analysis to the LAT data in 12 evenly divided energy bands in logarithm from 0.1–500 GeV. In the extraction, the spectral normalizations of the sources within 5 degrees from PSR J0614−3329 were set as free parameters, while all the other parameters of the sources were fixed at the values obtained from the above maximum likelihood analysis. We kept only spectral flux points when TS greater than 4 ($>2\sigma$ significance) and derived 95% flux upper limits otherwise. The obtained spectra are shown in Figure 3, and the fluxes and TS values are provided in Table 4. We found that while the offpulse emission was detected in an energy range of only <15 GeV, the onpulse emission from the pulsar was significantly detected in a high-energy range, upto approximately 200 GeV (see Table 4).

4.4. *Timing Analysis of >25 GeV data*

We performed timing analysis to the LAT data of PSR J0614−3329 to search for γ-ray pulsations at the high-energy range, for which we selected the minimum energy as high as possible but also ensured sufficient pulsation detection significance. We found the value of 25 GeV used in Ackermann et al. (2013) was proper. We first selected γ-ray photons within an aperture radius of 0.5 degrees from PSR J0614−3329, approximately corresponding to the 95% contamination angle of the incoming photons from a source. A total of ten photons were collected. Pulse phases for the photons were assigned using the updated ephemeris obtained in Section 4.1, and an H-test value of 30 was obtained, corresponding to 4.5σ detection significance (de Jager & Büsching 2010). These photons are shown in the top panel of Figure 4 according to their pulse phases, and the 0.1–500 GeV pulse profile is shown in the bottom panel of Figure 4 for comparison.

We then used a larger aperture radius of 2 degrees to include more photons (40 photons were collected), and weighted them by their probability of originating from the pulsar (calculated with using *gtsrcprob*). Pulse phases for these photons were assigned and a weighted H-test value of 48 was obtained (de Jager & Büsching 2010; Kerr 2011), corresponding to $\sim 6\sigma$ detection significance, indicating that the γ-ray pulsation from the source was significantly detected in >25 GeV energy band. We plotted the weighted photons in the middle panel of Figure 4 according to their pulse phases.

We also performed likelihood analysis to the >25 GeV data during the onpulse and offpulse phase intervals, with the emission from the source modeled with a simple power law. The γ-ray emission from PSR J0614−3329 was detected with TS$\simeq$ 65, having $\Gamma = 2.8\pm0.9$ and photon flux $F_{25-500} = 1.0 \pm 0.4 \times 10^{-10}$ photons s^{-1} cm^{-2} during the onpulse phase intervals. During the offpulse phase intervals, the γ-ray emission was not detected (TS$\simeq$ 0), and the derived 95% photon flux upper limit is 8×10^{-12} photons s^{-1} cm^{-2}. Two TS maps during these two phase intervals are shown in Figure 5. We ran *gtfindsrc* in the LAT software package to determine the position during the onpulse phase intervals and obtained R.A.=93.°53, Decl.= −33.°50, (equinox J2000.0), with 1σ nominal uncertainty of 0.°02. PSR J0614−3329 is 0.°01 from the best-fit position and within the 1σ error circle. The result confirmed the detection of pulsed γ-ray emission from photon folding.

5. DISCUSSION

5.1. *Spectral shape of MSPs*

Having analyzed approximately 7.5 yrs of *Fermi* LAT data for 39 MSPs reported in 2PC, we have obtained their spectra, which are all well described by a power law with exponential cutoff. We have thus determined their general spectral shape by fitting the spectra with such a function. Due to the intrinsic differences in their spectra, the allowed spectral shape region for MSPs is relatively large. However this spectral shape can be used to find candidate MSPs among the unidentified LAT sources. For example, using the criteria of >5 degrees, significant curvature in a spectrum, and non-variable, we (Dai et al. 2016) have found 24 such sources from the *Fermi* LAT third source catalog (Acero et al. 2015), but two of them, J0318.1+0252 and J2053.9+2922, likely have spectra not consistent with the spectral shape of MSPs because either Γ or E_c found for γ-ray emission of the two sources are not in the spectral shape range. Based on the known properties of the different types of LAT sources, they could be MSPs with quite different spectra or even other types of sources, for example the dark matter subhalo candidates as suggested by Bertoni et al. (2015). For the purpose of finding candidate MSPs and other types of unidentified γ-ray sources, searching through LAT sources at high Galactic latitudes by comparing their spectra with the spectral shape of MSPs we have determined is warranted.

5.2. *Pulsed γ-ray emission above 25 GeV from PSR J0614−3329*

High energy γ-ray emission is seen from 27 pulsars, as reported in the first *Fermi* catalog of sources above 10 GeV (Ackermann et al. 2013). Among them 20 sources were found to have pulsed γ-ray emission in >10 GeV

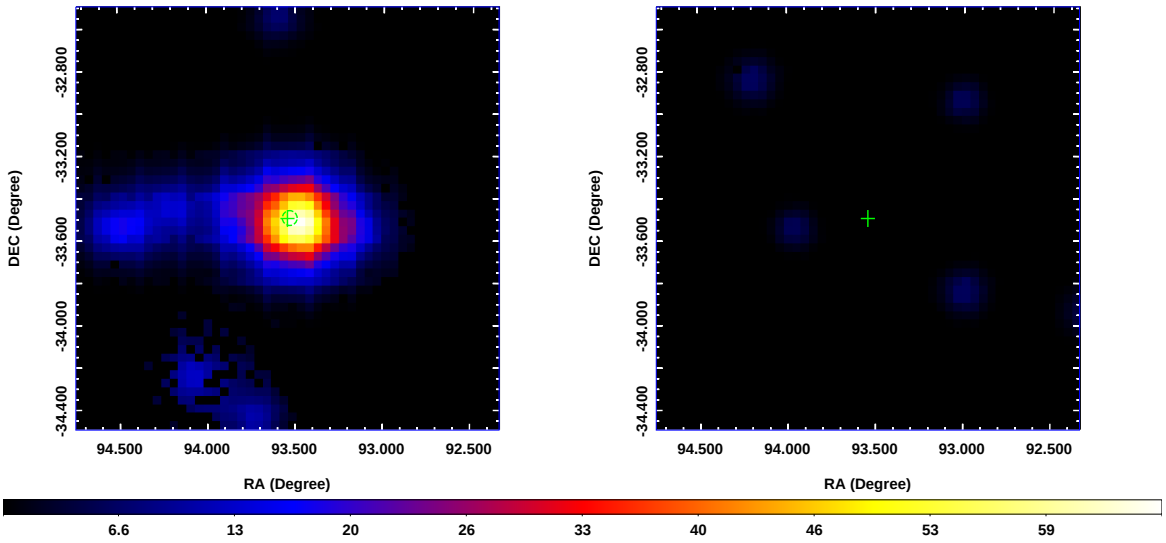

FIG. 5.— TS maps of a $2^o \times 2^o$ region centered at PSR J0614−3329 in the 25–500 GeV band, during the onpulse (*left* panel) and offpulse (*right* panel) phase intervals. The image scale of the maps is $0.^o04$ pixel^{-1}. The color bar indicates the TS value range. The green crosses mark the position of PSR J0614−3329. The green circle marks the 2σ error circle of the best-fit position obtained during the onpulse phase intervals.

band, including 17 young pulsars and 3 MSPs. Furthermore, PSR J0614−3329 was one of 12 pulsars found to have γ-ray pulsations in >25 GeV band, although it was only marginally detected in Ackermann et al. (2013). Our analysis, likely due to the longer time period of data (7.5 yrs vs. 3 yrs) and overall sensitivity improvement in the Pass 8 data, has shown that there is significant pulsed γ-ray emission upto 200 GeV from this MSP. The result has added PSR J0614−3329 to the group of the Crab and Vela pulsars that have been found to have >50 GeV pulsed emission (e.g., Harding & Kalapotharakos 2015 and references therein).

The mechanism of the very high-energy emission from pulsars remains to be solved. Currently the inverse-Compton scattering process in the outer magnetosphere or the pulsar wind region is considered to produce the pulsed emission detected in >10 GeV band from the Crab pulsar (see, e.g., Aleksić et al. 2011; Aharonian et al. 2012; Lyutikov 2013; Harding & Kalapotharakos 2015). Alternatively a non-stationary outer gap scenario has also been proposed recently (Takata et al. 2016), which has been used to interpret the >50 GeV pulsed emission from the Vela pulsar (Leung et al. 2014). In this scenario, the observed spectrum of a pulsar is the superposition of emission from the variable outer-gap structures. In Figure 3, we show the model fits to γ-ray emission from the Crab (Abdo et al. 2013; Aleksić et al. 2011) and Vela (Leung et al. 2014) pulsars (scaled by their 0.1–100 GeV total LAT fluxes respectively) for comparison. PSR J0614−3329 possibly has a stronger ∼200 GeV component than the Crab and Vela pulsars, although the large uncertainty does not allow a clear conclusion to be drawn. In order to investigate the emission process responsible for the high-energy component from PSR J0614−3329, detailed modeling (such as those in Harding & Kalapotharakos 2015; Takata et al. 2016) is needed.

This research made use of the High Performance Computing Resource in the Core Facility for Advanced Research Computing at Shanghai Astronomical Observatory. This research was supported by the Shanghai Natural Science Foundation for Youth (13ZR1464400), the National Natural Science Foundation of China for Youth (11403075), the National Natural Science Foundation of China (11373055), and the Strategic Priority Research Program "The Emergence of Cosmological Structures" of the Chinese Academy of Sciences (Grant No. XDB09000000). Z.W. acknowledges the support by the CAS/SAFEA International Partnership Program for Creative Research Teams.

REFERENCES

Abdo, A. A., Ackermann, M., Ajello, M., et al. 2010, ApJS, 188, 405
Abdo, A. A., Ajello, M., Allafort, A., et al. 2013, ApJS, 208, 17
Acero, F., Ackermann, M., Ajello, M., et al. 2015, ApJS, 218, 23
Ackermann, M., Ajello, M., Allafort, A., et al. 2013, ApJS, 209, 34
Aharonian, F. A., Bogovalov, S. V., & Khangulyan, D. 2012, Nature, 482, 507
Aleksić, J., Alvarez, E. A., Antonelli, L. A., et al. 2011, ApJ, 742, 43
Alpar, M. A., Cheng, A. F., Ruderman, M. A., & Shaham, J. 1982, Nature, 300, 728
Atwood, W. B., Abdo, A. A., Ackermann, M., et al. 2009, ApJ, 697, 1071
Bertoni, B., Hooper, D., & Linden, T. 2015, JCAP, 12, 035
Dai, X., Wang, Z., Jithesh, V., & Xing, Y. 2016, ArXiv e-prints
de Jager, O. C., & Büsching, I. 2010, A&A, 517, L9
Edwards, R. T., Hobbs, G. B., & Manchester, R. N. 2006, MNRAS, 372, 1549
Harding, A. K., & Kalapotharakos, C. 2015, ApJ, 811, 63
Hobbs, G. B., Edwards, R. T., & Manchester, R. N. 2006, MNRAS, 369, 655
Kerr, M. 2011, ApJ, 732, 38
Leung, G. C. K., Takata, J., Ng, C. W., et al. 2014, ApJ, 797, L13
Lyutikov, M. 2013, MNRAS, 431, 2580
Radhakrishnan, V., & Srinivasan, G. 1982, Current Science, 51, 1096

TABLE 1
Likelihood analysis results for 39 MSP targets

Source name	Γ	E_c (GeV)	F_{100} (10^{-12} erg cm^{-2} s^{-1})	TS
J0023+0923	1.3±0.2	1.9±0.5	7±1	447
J0030+0451	1.29±0.04	2.0±0.1	60±2	14973
J0034−0534	1.58±0.08	3.2±0.5	18±1	2117
J0101−6422	1.3±0.1	2.2±0.3	13±1	1835
J0102+4839	1.73±0.09	6±1	16±1	1259
J0218+4232	1.98±0.04	4.7±0.6	48±2	6417
J0340+4130	1.16±0.09	3.4±0.4	20±2	2274
J0437−4715	1.2±0.1	0.9±0.1	17±1	2830
J0610−2100	1.4±0.2	2.1±0.5	8±1	477
J0613−0200	1.42±0.07	2.9±0.3	31±2	2907
J0614−3329	1.38±0.02	4.9±0.2	112±2	33600
J0751+1807	1.4±0.1	3.6±0.7	13±1	1450
J1024−0719	1.2±0.3	2.2±0.7	4±2	213
J1124−3653	1.5±0.1	3.7±0.7	13±1	1088
J1125−5825	1.7±0.2	7±3	9±1	230
J1231−1411	1.09±0.03	2.4±0.1	100±2	28753
J1446−4701	0.7±0.4	1.7±0.6	5±1	249
J1514−4946	1.32±0.07	4.5±0.4	40±2	3831
J1600−3053	0.5±0.2	2.5±0.5	7±2	487
J1614−2230	0.8±0.1	2.0±0.2	25±2	2919
J1658−5324*	1.6±0.2	1.8±0.3	19±3	789
J1713+0747	1.5±0.2	3.2±0.8	10±1	578
J1741+1351	0.5±0.6	1.5±0.6	3±1	152
J1744−1134	1.53±0.07	1.8±0.1	39±2	2439
J1747−4036	1.2±0.2	2.3±0.5	9±1	274
J1810+1744	2.08±0.07	5±1	24±1	1853
J1823−3021A	1.1±0.2	3.3±0.6	10±1	496
J1858−2216*	0.4±0.3	1.4±0.2	9±2	626
J1902−5105	1.73±0.07	2.9±0.4	23±1	2502
J1959+2048	1.6±0.1	2.5±0.5	14±1	532
J2017+0603	1.07±0.08	3.8±0.4	34±2	4745
J2043+1711	1.57±0.06	4.9±0.6	29±1	3437
J2047+1053	1.3±0.4	3±1	4±2	152
J2051−0827	0.8±0.4	2.0±0.7	3±1	125
J2124−3358	0.85±0.07	1.8±0.1	38±2	7767
J2214+3000	1.13±0.06	2.1±0.2	32±2	6015
J2215+5135	1.2±0.1	3.6±0.7	12±1	817
J2241−5236	1.36±0.05	3.0±0.3	32±2	7167
J2302+4442	1.13±0.06	3.0±0.2	37±2	6157

The results for the sources marked with "$*$" were obtained in >0.2 GeV band.

Ray, P. S., Kerr, M., Parent, D., et al. 2011, ApJS, 194, 17
Takata, J., Ng, C. W., & Cheng, K. S. 2016, MNRAS, 455, 4249

TABLE 2
Spectral flux points for the MSP targets

	0.13 (GeV)	0.22 (GeV)	0.38 (GeV)	0.65 (GeV)	1.10 (GeV)	1.88 (GeV)	3.21 (GeV)	5.48 (GeV)	9.34 (GeV)	15.93 (GeV)	27.16 (GeV)
J0023+0923	2±1	–	2.2±0.5	2.2±0.3	2.3±0.3	2.0±0.3	0.5±0.2	–	–	–	–
J0030+0451	5±1	9.4±0.7	13.5±0.6	17.9±0.6	19.9±0.6	19.1±0.7	14.5±0.8	8.6±0.8	2.8±0.6	0.8±0.4	–
J0034−0534	2.2±0.9	3.4±0.5	4.4±0.4	4.8±0.4	4.8±0.4	5.2±0.4	4.1±0.4	2.3±0.4	1.5±0.4	–	–
J0101−6422	–	2.5±0.4	2.9±0.3	3.7±0.3	4.5±0.3	4.3±0.4	3.2±0.4	1.4±0.3	0.8±0.3	–	–
J0102+4839	4±1	4±1	3.5±0.6	3.3±0.4	3.9±0.4	4.6±0.4	3.5±0.4	2.8±0.5	1.6±0.4	0.9±0.4	–
J0218+4232	13±2	13±1	13.8±0.7	12.4±0.6	12.1±0.5	9.3±0.5	6.9±0.5	5.0±0.6	2.1±0.5	1.4±0.5	–
J0340+4130	–	–	3.0±0.5	3.9±0.4	5.6±0.4	6.3±0.4	7.3±0.5	4.8±0.6	3.7±0.6	0.7±0.4	–
J0437−4715	4.8±0.8	5.1±0.5	5.2±0.4	6.4±0.3	6.1±0.3	3.7±0.3	1.9±0.3	–	–	–	–
J0610−2100	–	3.0±0.7	1.5±0.4	2.5±0.3	2.5±0.3	2.3±0.3	1.3±0.3	1.3±0.3	–	–	–
J0613−0200	–	5±1	7.8±0.9	9.7±0.8	9.3±0.9	10.2±0.7	8.3±0.7	6.2±0.7	2.4±0.6	–	–
J0614−3329	8±1	11.7±0.6	16.0±0.5	21.7±0.6	27.9±0.7	32.9±0.9	34±1	28±1	19±1	9±1	4±1
J0751+1807	4.9±0.8	3.3±0.6	1.8±0.4	2.5±0.3	3.4±0.3	4.7±0.4	3.5±0.4	3.3±0.5	0.9±0.3	–	–
J1024−0719	–	–	1.0±0.3	–	1.5±0.2	1.3±0.2	1.3±0.3	0.7±0.3	–	–	–
J1124−3653	3±1	2.4±0.9	2.7±0.5	2.8±0.4	3.4±0.3	3.7±0.4	3.8±0.4	2.6±0.4	0.8±0.3	–	–
J1125−5825	–	–	–	3.4±0.7	3.0±0.5	1.6±0.4	2.7±0.5	2.1±0.5	–	0.9±0.5	–
J1231−1411	3±2	9.8±0.8	15.7±0.6	25.1±0.6	32.0±0.8	34.8±0.9	32±1	22±1	9±1	2.7±0.7	–
J1446−4701	–	–	–	1.3±0.4	1.9±0.3	2.5±0.3	2.1±0.4	0.8±0.3	0.7±0.3	–	–
J1514−4946	–	6±2	5.4±0.9	8.1±0.6	10.7±0.6	10.9±0.6	12.8±0.8	10.6±0.9	8.2±0.9	2.5±0.7	–
J1600−3053	–	–	–	–	2.1±0.3	2.6±0.3	2.9±0.4	2.4±0.4	1.7±0.4	–	–
J1614−2230	–	–	3.7±0.8	5.7±0.5	7.5±0.5	10.6±0.6	9.4±0.6	5.4±0.6	1.9±0.5	1.7±0.6	–
J1658−5324	–	2.9±0.4	5.8±0.9	6.0±0.6	6.3±0.5	4.5±0.5	2.8±0.4	1.5±0.4	–	–	–
J1713+0747	–	2.4±0.7	3.1±0.5	2.4±0.4	2.5±0.3	3.1±0.3	3.2±0.4	1.4±0.4	0.8±0.3	–	–
J1741+1351	–	–	–	0.9±0.3	1.3±0.3	1.2±0.3	1.7±0.3	0.6±0.2	–	–	–
J1744−1134	7±4	9±1	10.1±0.9	13.2±0.9	14.4±0.9	10.4±0.6	7.1±0.6	2.1±0.5	–	–	–
J1747−4036	–	3±2	3.5±0.8	3.0±0.6	3.2±0.5	2.4±0.4	2.7±0.4	1.5±0.4	–	–	–
J1810+1744	4±2	6.2±0.8	7.0±0.5	7.7±0.4	5.9±0.4	4.6±0.4	3.3±0.4	1.5±0.3	1.2±0.4	–	–
J1823−3021A	–	3±1	2.5±0.7	1.8±0.5	3.5±0.4	3.3±0.4	3.3±0.4	3.3±0.5	1.0±0.4	–	–
J1858−2216	–	–	–	–	2.7±0.4	3.4±0.4	4.3±0.4	3.8±0.4	1.5±0.4	0.9±0.3	–
J1902−5105	3.6±0.8	5.7±0.5	6.6±0.4	7.5±0.4	6.6±0.4	4.8±0.4	3.8±0.4	2.4±0.4	1.1±0.4	–	–
J1959+2048	–	–	3±1	5.2±0.7	4.8±0.6	4.3±0.5	2.9±0.4	1.2±0.3	–	–	–
J2017+0603	–	3.6±0.6	6.1±0.5	8.9±0.5	11.2±0.6	11.4±0.7	11.1±0.8	7.6±0.9	2.8±0.7	–	–
J2043+1711	3±1	5.1±0.7	5.5±0.5	6.3±0.4	8.2±0.5	7.3±0.5	7.9±0.6	5.9±0.6	3.6±0.6	1.1±0.5	–
J2047+1053	–	–	–	–	0.7±0.2	1.3±0.3	1.3±0.3	0.9±0.3	–	–	–
J2051−0827	–	–	–	–	1.3±0.3	0.9±0.2	0.8±0.2	0.9±0.3	–	–	–
J2124−3358	–	3.4±0.7	6.3±0.5	9.6±0.5	12.8±0.5	15.0±0.6	13.1±0.7	8.0±0.7	2.3±0.5	–	–
J2214+3000	–	4.8±0.6	6.1±0.5	9.0±0.4	10.7±0.5	11.4±0.5	8.8±0.6	6.7±0.6	1.3±0.4	–	–
J2215+5135	–	–	1.5±0.5	2.7±0.4	4.5±0.4	3.5±0.4	3.5±0.4	2.9±0.5	2.3±0.5	0.9±0.4	–
J2241−5236	3.4±0.9	5.3±0.5	6.4±0.5	7.8±0.4	10.5±0.4	9.7±0.5	9.8±0.6	5.9±0.6	3.0±0.6	–	1.3±0.7
J2302+4442	–	2.9±0.6	5.4±0.5	7.9±0.4	10.6±0.5	12.3±0.6	12.7±0.7	9.8±0.8	4.6±0.7	1.7±0.6	–

Fluxes are in units of 10^{-12} erg cm^{-2} s^{-1}.

TABLE 3
EXPONENTIALLY CUTOFF POWER-LAW FITS FOR PSR J0614−3329.

Data set	>0.1 GeV Flux (10^{-8} photon cm^{-2} s^{-1})	Γ	E_c (GeV)	b	TS
Total data	8.6 ± 0.2	1.38 ± 0.02	4.9 ± 0.2	1	33576
	8.2 ± 0.2	1.1 ± 0.1	1.6 ± 0.9	0.64 ± 0.09	33566
Onpulse data	19.1 ± 0.3	1.29 ± 0.02	5.1 ± 0.3	1	37013
	18.5 ± 0.4	1.1 ± 0.1	2.0 ± 0.9	0.68 ± 0.09	36997
Offpulse data	3.7 ± 0.2	1.42 ± 0.07	2.1 ± 0.2	1	3766

TABLE 4
Fermi LAT FLUX MEASUREMENTS OF PSR J0614−3329

		Total		Onpulse		Offpulse	
E (GeV)	Band (GeV)	$E^2dN(E)/dE$ (10^{-12} erg cm^{-2} s^{-1})	TS	$E^2dN(E)/dE$ (10^{-12} erg cm^{-2} s^{-1})	TS	$E^2dN(E)/dE$ (10^{-12} erg cm^{-2} s^{-1})	TS
0.14	0.1–0.2	8.5±0.7	276	17±1	310	4.8±0.8	63
0.29	0.2–0.4	13.8±0.5	1558	30±1	1868	6.4±0.5	265
0.59	0.4–0.8	20.8±0.5	5119	47±1	5536	8.8±0.4	865
1.20	0.8–1.7	28.8±0.6	9323	71±2	9877	9.6±0.5	1303
2.44	1.7–3.5	33.5±0.8	9731	88±2	10298	8.5±0.5	1013
4.96	3.5–7.1	30±1	5526	86±3	6301	4.0±0.5	259
10.08	7.1–14.4	17±1	1678	53±4	2045	1.1±0.4	30
20.50	14.4–29.2	7±1	333	23±3	439	0.3	0
41.70	29.2–59.5	0.6±0.5	6	2±1	10	0.9	0
84.79	59.5–120.9	0.6±0.6	6	2±2	8	1.2	0
172.42	120.9–245.9	2±2	5	8±6	9	2.5	0
350.62	245.9–500.0	3.8	0	14.3	0	5.1	0

Note: fluxes with uncertainties are given in energy bins with $>2\sigma$ detection significance, and fluxes without uncertainties are the 95% upper limits.